E15-2014-85

D. Testov [1,2], E. Kuznetsova [1], Yu. Penionzhkevich [1],
V. Smirnov [1], E. Sokol [1], D. Verney [2], J. Bettane [2],
S. Franshoo [2], F. Ibrahim [2], R. Li [2], I. Matea [2], B. Roussière [2],
I. Stefan [2], D. Susuki [2], K. Flanagan [3], B. Marsh [4]

THE ^{3}He LONG-COUNTER **TETRA** AT THE **ALTO ISOL** FACILITY

Submitted to «NIM A»

[1] Joint Institute for Nuclear Research, Dubna
[2] Institut de Physique Nuclaire, IN2P3/CNRS and University Paris Sud, Orsay, France
[3] University of Manchester, Manchester, United Kingdom
[4] CERN, Geneva, Switzerland

Тестов Д. и др. E15-2014-85

Нейтронный детектор TETPA для изучения осколков фотоделения на ALTO

Описывается новая установка (BEDO) для изучения свойств β-распада ядер, созданная на отводе масс-сепаратора PARRNe ускорительного комплекса ALTO. Производство нейтроноизбыточных ядер на ALTO обеспечивается за счет фотоделения урановой мишени при торможении электронного пучка. Установка оснащена лентопротяжной системой. Это позволяет получать источники радиоактивных ядер, представляющих интерес в самом центре модульной системы детектирования, а также осуществлять циклический перенос созданного источника за ее пределы. Механическая конструкция была разработана для реализации различных многодетекторных конфигураций в компактной геометрии. Описывается первый он-лайн эксперимент, выполненный на данной установке. Детектирующая система состояла из 80 ^{3}He счетчиков нейтронного детектора TETPA, созданного в ОИЯИ (Дубна), объединенных с HPGe и сцинтилляционным 4π-бета-детекторами. Эффективность регистрации нейтронов, измеренная с использованием источника ^{252}Cf, составила $(53 \pm 2)\%$. Эксперименты были выполнены на пучках ядер Ga, ионизированных лазером. Исходя из этих данных, измеренные в настоящей работе значения $P_n(^{82}\mathrm{Ga}) = (22{,}2 \pm 2)\%$ и $T_{1/2}(^{82}\mathrm{Ga}) = 0{,}604(11)$ с находятся в соответствии с литературными данными. В то же время измеренное значение $P_n(^{83}\mathrm{Ga}) = (84{,}8 \pm 3{,}6)\%$ подтверждает предположения о том, что ^{83}Ga является гораздо более сильным предшественником нейтронов, чем это считалось ранее.

Работа выполнена в Лаборатории ядерных реакций им. Г. Н. Флерова ОИЯИ.

Препринт Объединенного института ядерных исследований. Дубна, 2014

Testov D. et al. E15-2014-85

The ^{3}He Long-Counter TETRA at the ALTO ISOL Facility

A new β-decay station (BEDO) has been installed after the PARRNe mass-separator operated online to the electron-driven ALTO ISOL facility. The station is equipped with a movable tape collector allowing the creation of the radioactive sources of interest at the very center of a modular detection system and their cyclical evacuation outside of it. The mechanical structure was designed to host various assemblies of detectors in compact geometry. We report here the first online use of this system equipped by the ^{3}He neutron counter TETRA built at JINR, Dubna, associated with the HPGe and plastic 4π-beta detectors. The single neutron detection efficiency achieved is $(53 \pm 2)\%$ measured using ^{252}Cf source. The online commissioning of the TETRA was performed with a laser-ionized Ga beams. β and neutron events were recorded as a function of time. From this data we report $P_n(^{82}\mathrm{Ga}) = (22.2 \pm 2)\%$ and $T_{1/2}(^{82}\mathrm{Ga}) = 0.604(11)$ s in good agreement with values available in the literature. We also report $P_n(^{83}\mathrm{Ga}) = (84.8 \pm 3.6)\%$ measured by simultaneous β, neutron counting, which confirms that ^{83}Ga is much stronger neutron emitter than considered before.

The investigation has been performed at the Flerov Laboratory of Nuclear Reactions, JINR.

Preprint of the Joint Institute for Nuclear Research. Dubna, 2014

INTRODUCTION

Much effort is devoted to understand the role of neutron excess in the evolution of shell structure far from stability. One of the means to investigate nuclear structure is β decay. Once a nucleus is proven to exist, its β-decay properties, such as $T_{1/2}$, P_n (probability of β-delayed neutron emission) and others, which are relatively easy to measure by high-efficiency detectors, can provide the first hints on its structure. In addition, from the nucleosynthesis point of view, "waiting points" (nuclei on closed neutron shells) have significant effects on the rapid neutron capture-process (r process) dynamics and the abundance distribution. Reliable experimental $T_{1/2}$ and P_n values provide important inputs to r-process calculations. As it has been seen lately, most of the theories have failed to reproduce newly measured data sets near shell closures [1–4]. With new experimental data already (or shortly) available theoretical approaches can be adjusted.

The β-delayed neutron emission process can occur whenever the energy released in decay (Q_β) is larger than the neutron separation energy in the daughter nucleus and becomes significant if not the dominating decaying channel for neutron-rich nuclei far from stability. That is why usage of a proper neutron detector to study their properties is indispensable.

Neutron detection methods are based on registration of secondary charged particles produced as a consequence of neutron interaction with a detection media — the active material of the detector. Various media can be used resulting in many possible options for a neutron detector. Since a production rate of neutron-rich isotopes can be low, a high efficiency for the neutron registration can be considered as the key parameter. Thus, the cross section for a nuclear reaction

$$^3\mathrm{He} + n \rightarrow {}^3\mathrm{H} + {}^1\mathrm{H} + 765 \text{ keV} \tag{1}$$

is high in a thermal and low-energy neutron range [5]. Therefore, systems employing the ^{3}He detection media are known to provide uniformly high efficiency of neutron detection below 1 MeV ($\sim (40{-}70)\%$). Furthermore, since the detection of neutrons is based on a capture reaction, the ^{3}He detection arrays are

free from cross-talks allowing the possibility for neutron multiplicity measurements. It explains why the ^{3}He counters now are of arising interest for β-decay studies [6, 7].

We report in this paper on the installation and commissioning of the ^{3}He neutron counter TETRA [8] on the BEDO (BEta Decay studies at Orsay) [9] station. The performances and characteristics of the TETRA detector will be detailed in Sec. 1. We will describe the experimental conditions for the commissioning of the TETRA detector coupled to the BEDO station using laser ionized radioactive Ga beams at the PARRNe mass-separator operating online to the electron-driven ALTO ISOL facility. In the last Section, results on decay properties of ^{82,83}Ga, $T_{1/2}$ and P_n, obtained within this commissioning run, will be presented.

1. TETRA DETECTOR FOR ONLINE MEASUREMENTS AT ALTO

A description of the ALTO ISOL facility can be found in [10, 11]. At ALTO radioactive ion beams are available as mass-separated photo-fission fragments at the ion-source extraction voltage of 30 keV. Radioactive sources of interest are created by the interception of the beam by a movable Al-coated Mylar tape.

Ions are extracted from the source at low 30-keV potential with $1+$ charge state, mass separated, and implanted on an Al-coated Mylar tape. The BEDO mechanical frame was conceived to host various types of detectors positioned in compact geometry around the implantation point. In its neutron detection mode, the detector assembly comprises: $4\pi\beta$ plastics, HPGe detectors and 80 ^{3}He filled neutron counters. The geometrical arrangement of the detection array for the neutron detection mode, as shown in Fig. 1, was optimized to allow beam collection in the center of the array. The implantation point is located at the centre of the $\varnothing$13-cm cavity and is surrounded by 3-mm thick plastic scintillator (BC408) cylinder for beta detection, the set of ^{3}He neutron counters and tapered coaxial HPGe detector of the EUROGAM-1 type. The $4\pi\beta$ scintillator is linked to a photo multiplier tube located at 90° by a 50-cm light guide. The neutron counters are embedded in high-density polyethylene and are arranged in four rows, so that the distance between their centres is 5 cm. A layer of 15-cm thick borated polyethylene protects counters from background neutrons. Also there is a possibility to accommodate more counters in the 5th row as shown in Fig. 1.

The 4π neutron array TETRA was constructed at JINR [14]. It consists of 80 counters filled by ^{3}He at 7 atm with 1% admixture of CO_2, the active volume has 50 cm in length and $\varnothing$33 mm. Small diameter of the central cavity reassures almost 4π solid-angle coverage. TETRA is one of many neutron ^{3}He detectors built at JINR. Similar arrays were used in many experiments. For example,

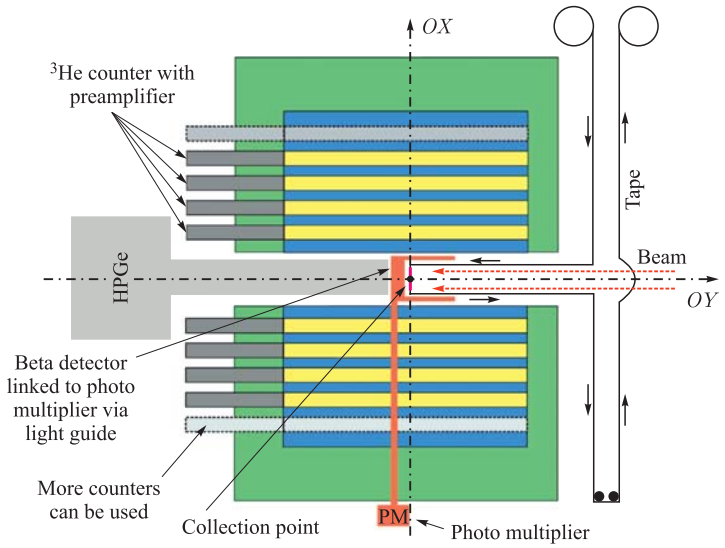

Fig. 1. Sectional view of the detection array optimized for neutron detection, including TETRA, at the BEDO tape station, see text for details

VASSILISSA (FLNR) neutron array [15–17] allows measurements of the neutron multiplicity, half-life of heavy and superheavy nuclei in spontaneous fission; SHIN experiment [8, 16] — to search for the best candidate for a superheavy element in nature via low-background measurements; FOBOS spectrometer and later miniFOBOS [18] — to study rare modes of spontaneous fission.

1.1. Design of the Electronic System. The TETRA electronic channels are grouped into six clusters with 16 channels each (one cluster is spare). Figure 2 shows a schematic diagram of the TETRA electronics for one cluster. Each counter in a cluster has a built-in preamplifier. Charged particles produced in the active volume in the nuclear reaction of Eq. (1) trigger signals which feed a preamplifier. Signals then further proceeded to a 16-channel amplifier. The gain for each channel is set individually via computer control by USB interface. The gain is adjusted so that signals at all outputs of the amplifier have the same amplitude. This allows discrimination of neutron signals from noises and γ by the low/high thresholds unified for all channels. All the events below the low threshold are rejected. Whereas response of the high threshold adds a special mark to the recorded data.

A typical pulse-height spectrum measured for one counter is presented in Fig. 3. The low-energy peak corresponds to ionization produced by γ-rays; whereas the neutron full-energy peak corresponds to detection of both particles produced in the neutron-capture reaction Eq. (1); the low energetic plateau be-

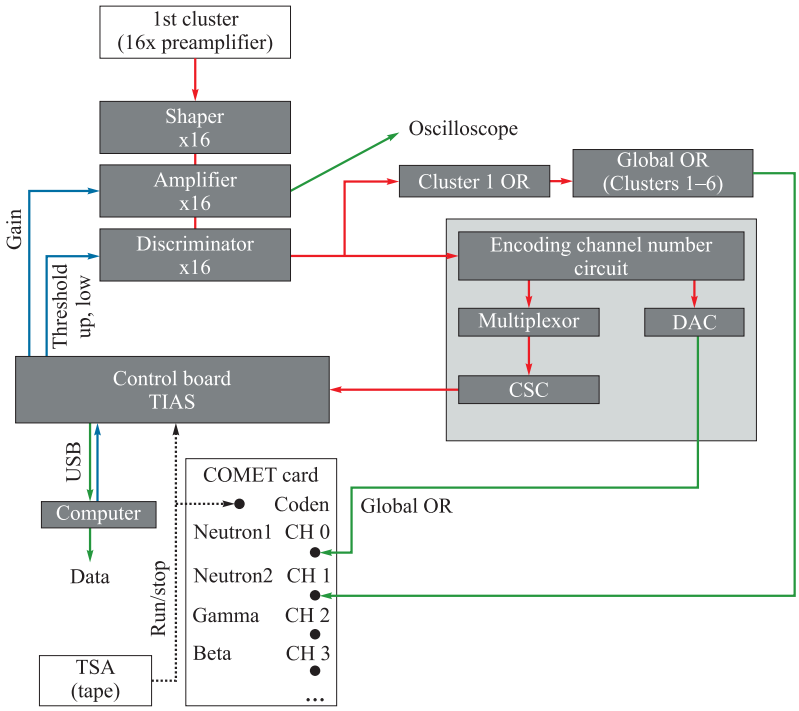

Fig. 2. Diagram for the TETRA electronic system providing neutron data in a stand-alone mode and being coupled with the COMET data acquisition system at BEDO. Synchronization is thanks to the «coden enable» signal generated by the Tape Station Automate (TSA) (see text for details). For the sake of clarity only one TETRA cluster is shown

tween them is due to the wall effect (only one of the two particles is detected due to the kinematic of the reaction, or a counter wall does not allow full energy disposal); finally, some high-amplitude events are largely due to alphas and sparks.

On the one hand, amplitude signals from the discriminator are transformed into the logic ones via the OR scheme and directly connected to the COMET data acquisition card. On the other hand, signals from the discriminator also feed Encoding Channel Number Circuit (ECNC) which serves Multiplexor and Digital to Amplitude Converter (DAC) providing a plateau voltage which height proportional to the identification number of the counter fired.

The Multiplexor is a part of TETRA Integrated Acquisition System (TIAS) which can be used independently, coupled or in parallel with COMET. Multiplexor can hold up to 16 channels even fired simultaneously, that is why the dead time of TIAS is negligibly small. It allows the correct registration of neutron events of high multiplicity. The Multiplexor transmits neutron events subse-

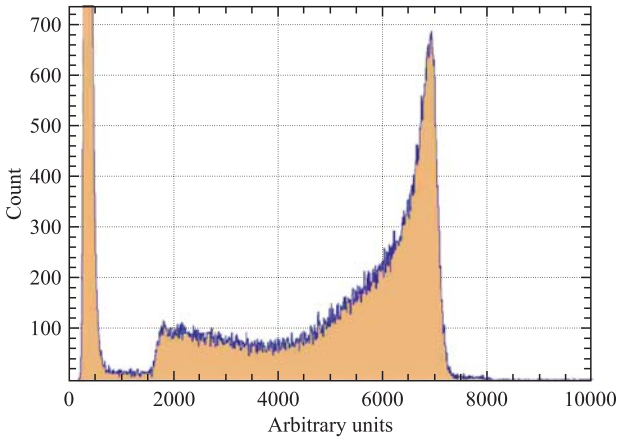

Fig. 3. A typical pulse-height spectrum recorded for one counter with an AmBe source

quently to the Control Board via Convertor to the Serial Code (CSC). The time is defined by a timer counter with a 20-byte ($\sim$ 2 s) capture register. At overflow the time counter is reset to 0 with a stamp in the recorded data. Thus, when a channel is touched, time and a high threshold mark are captured by a computer via USB interface.

COMET is a triggerless acquisition card used presently at ALTO. It allows one to proceed data with six detectors determining the energy (coded on 13 bits (8192 cx)) and the time (coded on 47 bits — 15.6 h) of signals from detected radiations. Part of the processing is done in the card itself using a 32-bits DSP, 40 MHz [19]. In our experiments, as shown in Fig. 2, two signals from TETRA were recorded. The signal noted "Neutron1" was the identification number of the fired counter with its associated time. However, the occupation time of this channel for the coding and readout of the identification information was 25 μs, thus eliminating the possible registration of neutron events of multiplicity higher than 1. For that reason this channel was not considered in the analysis. The signal "Neutron2" was the OR time signal without any energy information (no amplitude coding) which limited the occupation time of the COMET channel to 10.3 μs. However, all neutron data, including time, number of counter fired, and a high threshold mark were recorded by TIAS in parallel. Signals from HPGe and $4\pi\beta$ detectors, processed by typical electronic analog circuits, were plugged into CH2 and CH3 COMET inputs, respectively. The "coden" signal, generated by Tape Station Automate (TSA) connected to COMET and TIAS, allowed their synchronization and data recording interruption during the tape motion.

1.2. Neutron Life-Time in the Detector. Neutron life-time in the detector τ is determined by moderation and diffusion times and can be estimated via a

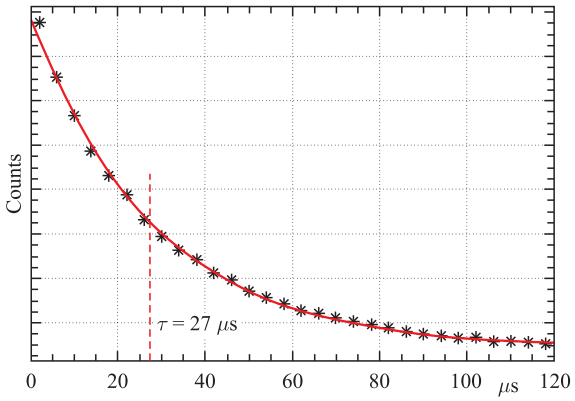

Fig. 4. Time difference between two consecutive neutrons emitted in spontaneous fission of ^{252}Cf (see text for details)

neutron time distribution relative to a start signal, Fig. 4, which shows a time difference distribution between two consecutive neutrons emitted in spontaneous fission of ^{252}Cf. The neutron life-time $\tau = (28.2 \pm 0.2)\ \mu$s was obtained from a fit $(\exp(-t/\tau) + \text{const})$ and is defined as a time to detect half of the neutrons.

1.3. Efficiency. The TETRA efficiency* was found by the method based on neutron multiplicity distribution emitted from a source proposed in [20]. This method was also used previously by our group [21].

Prompt spontaneous fission neutrons of ^{252}Cf are described by the average number of neutrons per decay ($\bar{\nu} = 3.75$ [22,23]) and by multineutron emission probabilities P_l, $l = 0, 1, 2 \ldots l_{\max}$. For a detection efficiency (ε_0) below 100% the observed multiplicity distribution is different from the real one. Under the assumption that neutrons are detected independently the probability to detect n neutrons F_n is the sum of the partial probabilities to detect the emission of $\nu = n, n+1, \ldots, \nu_{\max}$ neutrons:

$$\sum_{\nu=n}^{\nu_{\max}} K_{n\nu} P_\nu = F_n, \quad n = 1, 2, \ldots, n_{\max}, \tag{2}$$

where P_ν are the components of the true neutron distribution; $\nu_{\max}$ is the maximum possible number of neutrons per fission; $K_{n\nu}$ is the matrix of the transmission coefficients between real and measured components. The exact solution of Eq. (3) is given in [20]:

$$K_{n\nu} = \frac{\nu!}{n!(\nu - n)!} \varepsilon^n (1 - \varepsilon)^{\nu - n}. \tag{3}$$

*For single neutrons.

If N_i and N_j are the numbers of events detected with i and $j \neq i$ neutrons emitted in the same number of decays $N_{\rm dec}$, considering Eqs. (2) and (3):

$$N_i = N_{\rm dec} \cdot F_i = N_{\rm dec} \sum_{\nu=i}^{\nu_{\max}} \frac{\nu!}{i!(\nu-i)!} \varepsilon^i (1-\varepsilon)^{\nu-i} P_\nu. \quad (4)$$

N_j can be expressed analogically to Eq. (4). Therefore, their ratio N_i/N_j is a function of an efficiency ε:

$$\frac{N_i}{N_j} = \frac{F_i}{F_j} = f(\varepsilon). \quad (5)$$

Comparing the experimentally measured multiplicity ratios N_i/N_j to the calculated F_i/F_j ones, $\epsilon_0 = (53 \pm 2)\%$ was found. The obvious advantage of the method is independence of the initial measurements of neutron activity of a source provided with its passport. Furthermore, the method leads to self-check procedure: whatever an efficiency is measured, multiplicity ratios must justify the calculated multiplicity ratios unless there is an electronic problem or a mistake in the analysis.

1.4. The MCNP Simulations for TETRA. To optimize the installation of TETRA on the BEDO tape station, a validated computer model of TETRA was highly needed. This model was created using the MCNP code (Monte Carlo N-Particle transport) [24]. The MCNP code is a well-established powerful tool for neutron-transport calculations initially aimed at reactor calculations but widely used nowadays for varied applications showing good agreement with experimental data.

Figure 5 presents the calculated and measured efficiency of the TETRA array for a ^{252}Cf source moved inside the detector on the beam axis OY (see Fig. 1).

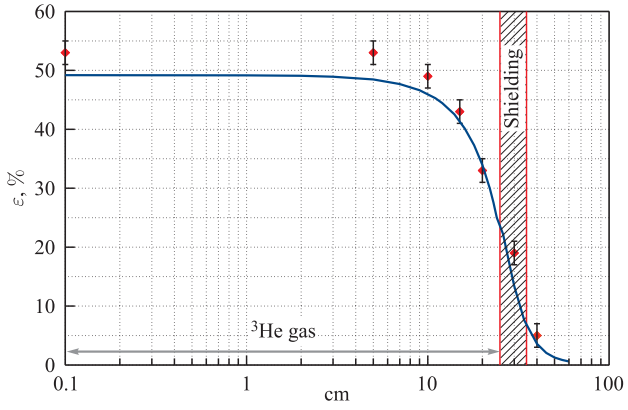

Fig. 5. Validation of the model: calculated and measured efficiency of TETRA as a function of distance of ^{252}Cf source from the center of the detector

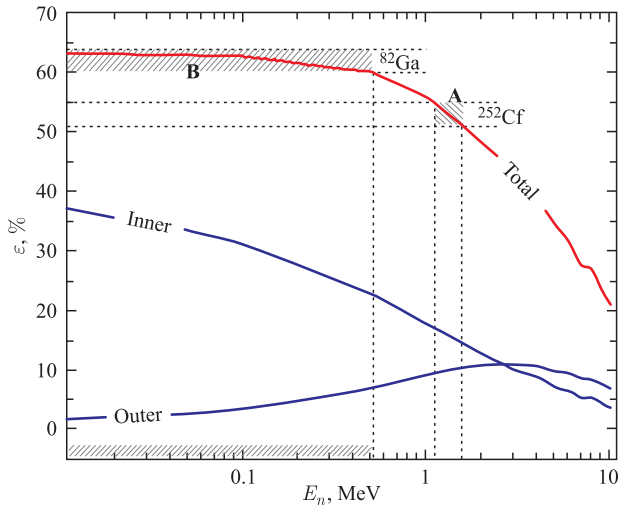

Fig. 6. The MCNP-calculated total efficiency of TETRA (red solid line) and MCNP-calculated efficiencies of the inner and the outer layers of counters (blue solid lines) as a function of neutron energy. Hatched interval **A** shows the measured efficiency for ^{252}Cf spontaneous fission neutrons and **B** stands for Ga β-delayed neutrons

As can be seen, the efficiency is obviously maximum at the center and is almost flat up to 8-cm shift from the center, gradually falling down with further increase of the distance from the center. The calculated curve slightly underestimates the experimental points, which is a consequence of uncertainty in density of materials used and geometrical dimensions of parts of the detector. The TETRA model developed is fully discussed in [25].

As seen from Fig. 6, illustrating the calculated efficiency of TETRA as a function of neutron energy, the efficiency is high and is almost constant up to 0.8-MeV neutron energy. The efficiency ε_0 measured by the method described above for prompt neutrons from spontaneous fission of ^{252}Cf source is shown by hatched area **A**. The $\varepsilon_{\rm tetra}$ measured for β-delayed neutrons from a radioactive source in the experiments described in Subsec. 2.3 is shown by hatched area **B**. As can be seen, the energy of β-delayed neutrons detected was lower than the energy of prompt neutrons.

2. EXPERIMENTS

Ions of Ga^{+1} were extracted with the Resonant Ionization Laser Ion Source (RILIS) using two-step ionization scheme [12] at 30-keV energy towards the online isotope separator PARRNe [13]. The pure beam was then transmitted to the BEDO station. All the γ transitions in the recorded γ spectra were identified and no impurities were observed for ^{82,83}Ga settings.

During these experiments Ga nuclei were collected onto a Mylar tape at the centre of the detection array. Typical decay chains following the decay of the collected nuclei are shown in Fig. 7. In order to enhance shortest lived activities, the sources were evacuated outside the detection array by moving the tape with a period depending on a half-life in the decay chain of the particular Ga isotope studied. The TIAS and the COMET recorded data between two consecutive tape movements triggered by the TSA signal, which stopped/opened the DAQs when the tape was moving. A short counting time of $T_{\rm bg}$ was allowed before each beam collection to estimate the evolution of the background during experiments, Fig. 8. After irradiation during $T_{\rm beam}$, the beam was stopped to measure the activity of the accumulated radioactive source for a duration of $T_{\rm decay}$. Afterwards, the tape was moved for 2 m to remove the source outside the detection array.

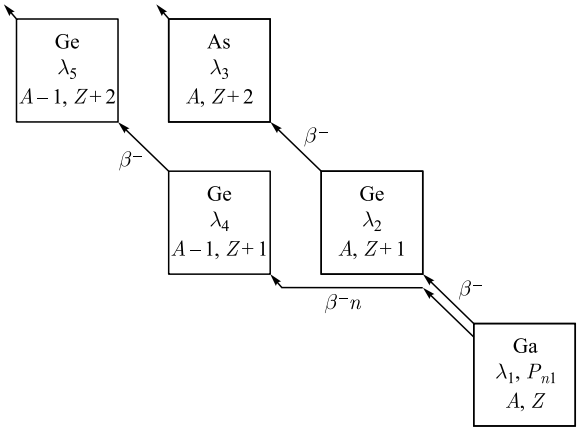

Fig. 7. The β^- and $\beta^- n$ decay chains of Ga radioactive sources; λ_i ($i = 1 \ldots 5$) are decay constants; P_{n1} is probability of β-delayed neutron emission of Ga

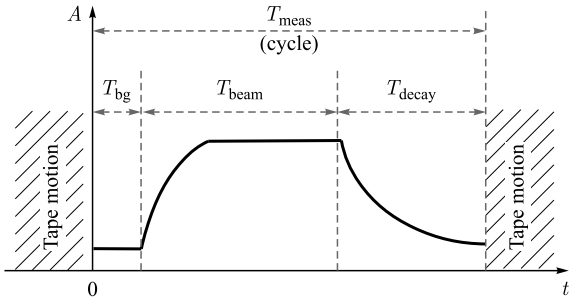

Fig. 8. The $\gamma-\beta-n$ activity is recorded by DAQs only during $T_{\rm beam}$, which consists of background measurements $T_{\rm bg}$, irradiation during $T_{\rm beam}$ and decay for $T_{\rm decay}$. At the end of each cycle time is reset

2.1. Measurements of P_n Value. The P_n value of a neutron precursor (A, Z) is the ratio between the number of neutrons emitted and the total number of β decays. There are different general methods to experimental determination of P_n. These approaches differ in a way mother/daughter nuclei are counted [26]. In the present experiments, β and neutron activity curves were measured. Collected simultaneously, β and neutron integrals were used in the analysis based on solutions of Bateman equations [27]. It allowed one to separate contributions of isotopes in β^-, $\beta^- n$ decay chains, Fig. 7.

The decay of a radioactive source created by accumulation of beam depends on both decay constants λ_i and P_{n1}, Fig. 7. In case of ^{82,83}Ga multineutron emission probabilities can be neglected due to small $(Q_\beta - S_{2n})$ energy window. Also negative $(Q_\beta - S_{1n})$ energy window for Ge leads us to an assumption that Ga isotopes are the only unique neutron precursors on their decay chains. Therefore, a number of ith nuclei accumulated at t moment during the implantation $N_i^{\rm col}(t)$ is characterized by the set of coupled linear differential equations:

$$\begin{cases} \frac{{\rm d}N_1(t)}{{\rm d}t} = -\lambda_1 \cdot N_1(t) + \phi, & (A, Z), \\ \frac{{\rm d}N_2(t)}{{\rm d}t} = -\lambda_2 \cdot N_2(t) + (1 - P_{n1}) \cdot \lambda_1 N_1(t), & (A, Z+1), \\ \frac{{\rm d}N_3(t)}{{\rm d}t} = -\lambda_3 \cdot N_3(t), & (A, Z+2), \\ \frac{{\rm d}N_4(t)}{{\rm d}t} = -\lambda_4 \cdot N_4(t) + P_{n1} \cdot \lambda_1 N_1, & (A-1, Z+1), \\ \frac{{\rm d}N_5(t)}{{\rm d}t} = -\lambda_5 \cdot N_5(t) + \lambda_4 N_1(t), & (A-1, Z+2), \end{cases} \tag{6}$$

where ϕ is the production rate of Ga; P_n is its probability of β-delayed neutron emission and λ_1 is its decay constant; λ_{2-5} are decay constants of its decay daughters. The number of ith nuclei accumulated at t moment during the implantation $N_i^{\rm col}(t)$ is found as a solution of Eqs. (6) with initial condition $N_i^{\rm col}(0) = 0$. The number of ith nuclei at t moment during the decay $N_i^{\rm dec}(t)$ is given by solution of Eqs. (6) at $\phi = 0$ and with initial conditions $N_i^{\rm dec}(t) = N_i^{\rm col}(T_{\rm beam})$. The analytical solutions for $N_i^{\rm col}(t)$ and $N_i^{\rm dec}(t)$ are too cumbersome, but are easily obtained using any computer application for numerical computations. Therefore, the total number of decayed nuclei $\sum_{i=1}^{5} A^{\rm tot}$ is defined by summing two integrals over the implantation and decay correspondingly:

$$A^{\rm tot} = \sum_{i=1}^{5} \left(\int_0^{T_{\rm beam}} \lambda_i \cdot N_i^{\rm col}(t) dt + \int_{T_{\rm beam}}^{T_{\rm meas}} \lambda_i \cdot N_i^{\rm dec}(t) dt \right). \tag{7}$$

In fact, since all the nuclei in the region have 100% β-decay mode, it is reasonable to assume that the number of decays is equal to the number of β emitted. As a result, a total number of betas $N_\beta^{\rm exp}$ and neutrons $N_{\rm neutron}^{\rm exp}$ detected in an experiment corrected by beta $N_\beta^{\rm bg}$ and neutron $N_{\rm neutron}^{\rm bg}$ background events

and detection efficiencies ϵ_β, $\epsilon_{\rm neutron}$, respectively, is described by Eq. (8):

$$\begin{cases} (N_\beta^{\rm exp} - N_\beta^{\rm bg})\frac{1}{\epsilon_\beta} = \int\limits_0^{T_{\rm meas}} A_\beta^{\rm tot}(t), \\ \\ (N_{\rm neutron}^{\rm exp} - N_{\rm neutron}^{\rm bg})\frac{1}{\epsilon_{\rm neutron}} = \int\limits_0^{T_{\rm meas}} A_{\rm neutron}^{\rm tot}(t). \end{cases} \tag{8}$$

If all the decay constants λ_i are known, Eqs. (8) are solved analytically for P_{n1} and ϕ. To determine uncertainties on P_{n1} and ϕ, the parameters entering Eqs. (8) (λ_i) were varied within the uncertainties quoted in the literature and had a negligible effect on the final result. The major contribution to error on P_{n1} and ϕ was due to statistics of measured β and neutron integrals. To verify values of P_{n1} and ϕ obtained this way, a fit of β and neutron activity curves was performed using the ROOT system [28]. The fit functions were set in an analytical way, with P_{n1} and ϕ as free parameters with initial values given by solution of Eqs. (8). The decay constants were fixed at the given values. The parameter minimization and error analysis were performed with MINUIT packages built in ROOT.

2.2. $\gamma{-}\beta{-}n$ **Coincidence Technique.** We have explored the possibility to obtain γ-spectra gated by both β and neutron emissions. It is the first time such results are available in the case of ^{82,83}Ga decays. The typical β–γ coincidence window was 0.1 μs, whereas due to long neutron diffusion time the γ–β–n coincidence window was 128 μs. Random contribution in the peak areas in $\gamma{-}\beta$-gated spectra was considered. Random coincidence counting rate $r_{\gamma-\beta}$ was estimated by $r_{\gamma-\beta}[{\rm s}^{-1}] = S_\beta^{\rm peak}[{\rm s}^{-1}] \cdot N_\beta[{\rm s}^{-1}] \cdot T_{\rm window}[{\rm s}]$. $T_{\rm window}$ is the duration of the coincidence window, $S_\beta^{\rm peak}$ is the counting rate in the peak surface in the β-gated γ-spectrum; and N_β is the β counting rate. The random coincidence contribution in the peak surface obtained was as low as 0.1%. In the same manner, random coincidence for $\gamma{-}\beta{-}n$-gated spectra was estimated to be at the level 3–5% due to larger neutron coincidence window (128 μs).

2.3. TETRA Efficiency for β-Delayed Neutrons. The efficiency of TETRA for prompt neutrons with average energy of ~ 2.348 MeV [29] of spontaneous fission of ^{252}Cf was measured as described above to be $\sim 52\%$. However, based on numerous experimental evidence [30–34], the energy of β-delayed neutrons is generally considered to be below 1 MeV. Obviously, the energy information provided with a neutron detector such as TETRA is very poor. However, as proposed by Reeder et al. [33], by mapping the counters fired it is possible to restore the initial neutron energy: less energetic neutrons are detected by the inner layer of counters; whereas more energetic ones require a longer path to become thermal and touch the outer layer of counters. As seen from comparison

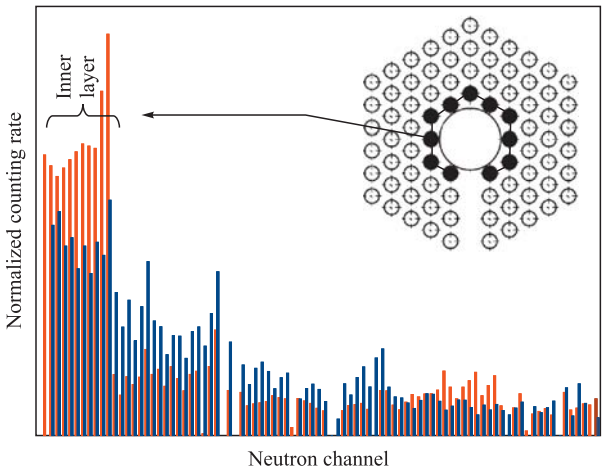

Fig. 9. Normalized neutron counting rate per counter for Ga β-delayed neutrons (in red) as compared to prompt fission neutrons of ^{252}Cf (in blue). TETRA is schematically shown illustrating the position of the inner counters

of the normalized counting rate per TETRA neutron counter, Fig. 9, the response of the inner layer of counters is significantly higher for β-delayed neutrons of Ga rather than for prompt fission neutrons of ^{252}Cf. Therefore, the conclusion is that delayed neutrons are less energetic (than the prompt ones). This fact results in the higher detection efficiency for β-delayed neutrons. The TETRA efficiency used in the analysis for masses $A = 82$ and 83 was $(63 \pm 5.6)\%$ and $(60.5 \pm 1.2)\%$, respectively, measured as weighted average from ratios of corresponded peak areas in $\gamma-\beta$–neutron ($S_{\gamma-\beta-\mathrm{neutron}}$) and $\gamma-\beta$ ($S_{\gamma-\beta}$) coincidence spectra:

$$\epsilon_{\mathrm{tetra}} = \frac{S_{\gamma-\beta-\mathrm{neutron}}}{S_{\gamma-\beta}} \cdot \frac{1}{(1 - DT_{\mathrm{neutron}})}, \tag{9}$$

Table 1. Ratio of peak areas of the most intense transitions in ^{82}Ge observed in β–neutron-gated γ-spectrum and in β-gated–γ-spectrum

E_γ, keV	Ratio
1365.41	0.62(7)
1176.1	0.53(7)
938.83	0.56(3)
867.2	0.59(14)
1348	0.60(1)

where $DT_{\mathrm{neutron}} < 0.01\%$, dead time of the neutron electronic channel, can be neglected. The measured efficiency corresponds to neutrons below 500 keV, Fig. 6. Thus, neutrons detected were mostly of low energy. In Fig. 10, γ is presented as a spectrum measured for $A = 83$. In β-gated γ-spectrum (top, blues) transitions from daughters nuclei (^{82,83}Ge, ^{82,83}As, ^{82,83}Se) are presented. Whereas in the β–neutron-gated

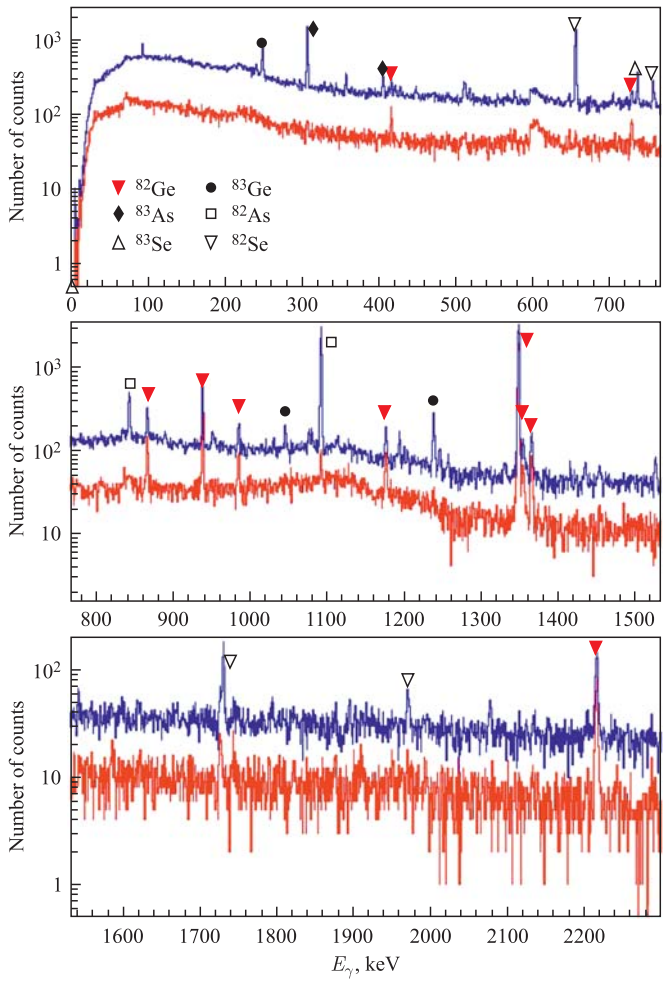

Fig. 10. Measured $\gamma-\beta$-gated (in blue) and $\gamma-\beta$–neutron-gated (in red) spectra recorded for mass $A = 83$. In the latter, the strongest transitions belong only to decay of ^{83}Ga$\xrightarrow{\beta-n}$ ^{82}Ge. Marked transitions are in daughters nuclei

γ-spectrum (bottom, red) only transitions characterizing ^{83}Ga $\xrightarrow{\beta-n}$ ^{82}Ge decay are seen. The ratios of surfaces of the most intense transitions in ^{82}Ge in both spectra are listed in Table 1.

3. RESULTS

3.1. The $\beta-n$ Decay of ^{82}Ga. Half-life and probability of β-delayed neutron emission for ^{82}Ga were already measured several times and should be well

established [35–38]. That is why ^{82}Ga is considered for this commissioning experiment.

All neutrons detected for $A = 82$ were attributed either to background or to $^{82}\text{Ga} \xrightarrow{\beta-n} {}^{81}\text{Ge}$ decay. It is due to the fact that β-delayed neutron emission is not energetically favourable for the other isotopes in $A = 82$ isobaric chain and thanks to the high purity of the beam. The adopted half-life $T_{1/2}(^{82}\text{Ga}) = 0.604(11)$ s found as a result of the fit of the growth pattern for the recorded neutron activity, Fig. 11, is compatible with other experiments, Fig. 12.

The background was considered constant at the level measured within 100 ms prior to 2-s implantation time and was accepted to be a constant. Total neutron and

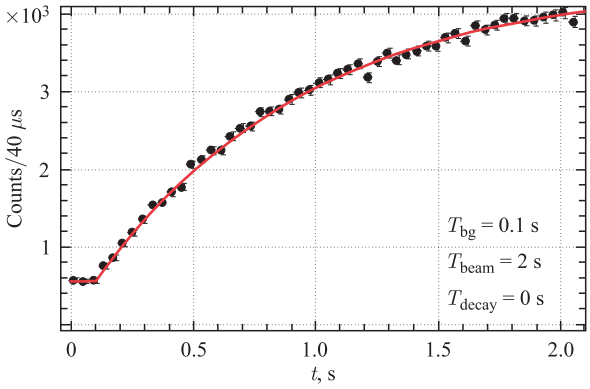

Fig. 11. Recorded neutron activity (dots) from the accumulation of the ^{82}Ga beam onto the tape and corresponding fit (line)

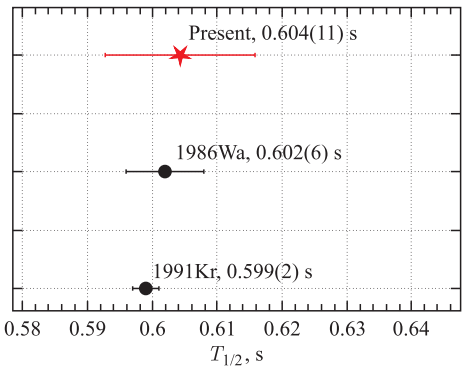

Fig. 12. $T_{1/2}$ of ^{82}Ga presently measured by recorded neutron activity (in red star) in comparison with other works: 1986Wa [36]; 1991Kr [38]

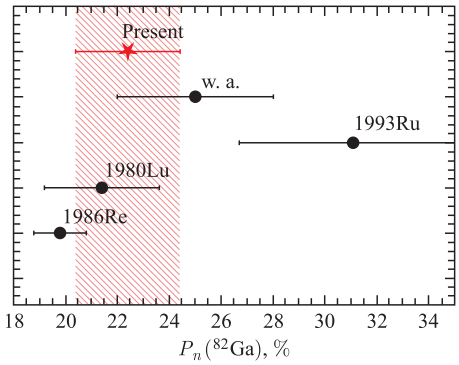

Fig. 13. Presently measured P_n for ^{82}Ga (in red star) comparing to other data: 1993Ru [35]; 1986Re [36]; 1980Lu [37] with w.a. as the weighted average

β integrals, corrected by background conditions and detection efficiencies, were input parameters to the Bateman equation (6) specified for the ^{82}Ga case. The $T_{1/2}$ of ^{82}Ga derived from our neutron activity curve was used. The decay parameters of the daughters nuclei were taken from literature. Varying these parameters within the uncertainty quoted had a negligible effect on solution of Eq. (6). The errors on the solution of the system (ϕ, P_n) were mainly determined by collected neutron and β statistics. P_n (^{82}Ga) = 22.2(2.0)% and $\phi(^{82}\mathrm{Ga}) = 1.29(6)\cdot 10^3$ s^{-1} were obtained. P_n also agrees well within error bars with the weighted average from previously data quoted in literature, Fig. 13.

3.2. The $\beta-n$ Decay of ^{83}Ga. For mass $A = 83$ all detected neutrons were attributed either to background or to $^{83}\mathrm{Ga} \xrightarrow{\beta-n} {}^{82}\mathrm{Ge}$ decay. Although, neutron emission is energetically possible for ^{83}Ge and ranged from 0.01% to 2% in different predictions [26, 46], growth and decay pattern for the recorded neutron activity correspond to a half-life of 0.312(1) s, Fig. 14. It coincides well with a half-life of ^{83}Ga quoted in literature, Fig. 15. Therefore, even if β-delayed neutron emission from ^{83}Ge took place, it was neglected.

The pattern of 100-ms background measurements prior to 3 s of implantation of isotopes followed by 2 s of decay was used for ^{83}Ga. The total neutron and β integrals, corrected from background conditions and detection efficiencies, were input parameters for the Bateman equation (6) specified for the ^{83}Ga case. The $T_{1/2}$ of ^{83}Ga derived from the neutron activity curve was used. The decay parameters of the daughters were taken from literature. Varying these parameters within the uncertainty quoted had a negligible effect on solution of Eq. (6). The errors on the final were mainly determined by collected neutron and β statistics. Values of P_n (^{83}Ga) = 84.8(3.6)% and $\phi(^{83}\mathrm{Ga}) = 370(10)$ s^{-1} were obtained.

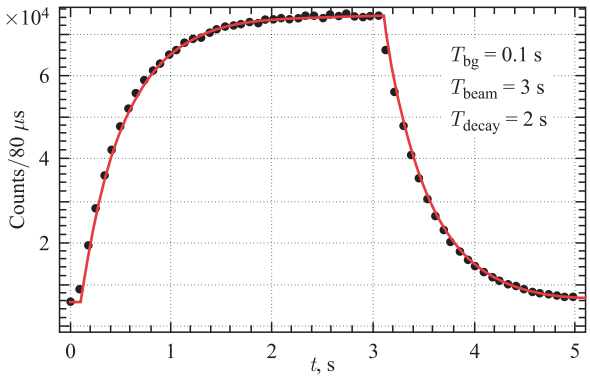

Fig. 14. Recorded neutron activity (dots) from the accumulation of the ^{82}Ga beam onto the tape and corresponding fit (line)

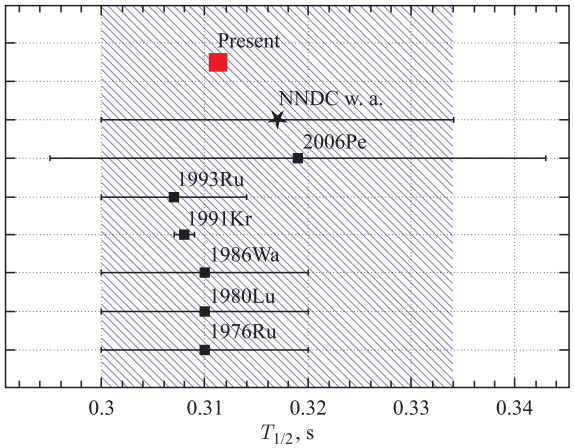

Fig. 15. Presently measured $T_{1/2}$ of ^{83}Ga by recorded neutron activity curves (red square) in comparison with other works: 2006Pe [47]; 1993Ru [35]; 1991Kr [38]; 1986Wa [36]; 1980Lu [37]; 1976Ru [48]; NNDC w.a. — the weighted average as is in NNDC [39]

Discrepancy of experimental P_n values of ^{83}Ga ranges from $\sim 14.9(18)\%$ [35] to 62.8(25)%, the most recent one (Winger et al. [44]), see also Table 2 and Fig. 16. Winger et al. highlighted that their value is 4.2 times larger than probably the best previous measurements [35], and is underestimated by the continuum quasiparticle random-phase approximation [3]. As noticed, application of the blocking approximation with the standard density functional [45] gives an increase in β-delayed neutron emission probabilities and agrees much better with their data. Unfortunately, due to the lack of measurements of absolute branching

Table 2. List of measured and predicted $T_{1/2}$ and P_n for ^{83}Ga

$T_{1/2}$, s	P_n, %	Method	Reference
Experiment			
0.308(1)	84.8(3.6)	n	Present
	62.8(2.5)	γ	Winger et al. [44]
0.319(24)	—	γ	Perru et al. [47]
0.307(7)	14.9(18)	n	Rudstam et al. [35]
0.308(1)	—	n	Kratz et al. [38]
0.310(10)	54(7)	n	Warner et al. [36]
0.31(1)	43(7)	n	Lund et al. [37]
0.308(4)	62.8(63)	n	Rudstam et al. [48]
Macroscopic statistical models			
0.091	46.73	Gross	Tachibana [43]
0.082	33.79	KHF	Pfeiffer [46]
Microscopic shell models			
0.239	64.52	GT	QRPA 1997, Möller [26]
0.327	59.10	GT	QRPA 2002, Möller [41,42]
0.20	15	GT + FF	CQRPA 2005, Borzov [3]
0.35	39	GT + FF	CQRPA 2012, (blocking) Borzov [45]
0.35	50	GT + FF	CQRPA 2012, (no blocking) Borzov [45]

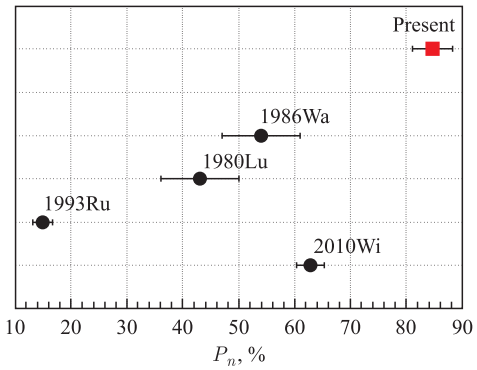

Fig. 16. Presently measured P_n of ^{83}Ga (in red square) in comparison with the known data: 1993Ru [35]; 1986Wa [36]; 1980Lu [37], 2010Wi [40]

ratios (I_β) to levels of ^{83}Ge, the authors admit that the P_n value they obtain depends on their estimations of I_β, which has to be verified independently.

Our $P_n(^{83}\text{Ga})$ value is independent of estimations of absolute branching ratios and is 5.7 times higher than measurements in [35], which confirms the tendency pointed out by Winger et al. that ^{83}Ga is much stronger neutron emitter than considered before.

4. SUMMARY

The 4π high-efficiency neutron detector TETRA built at JINR, Dubna, has been modified enabling measurements of β-decay properties of neutron-rich nuclei produced at recently inaugurated ISOL facility ALTO (Orsay). The unique design of the detection system was imposed by a requirement to have a constant neutron efficiency high up to 1 MeV and the necessity to simultaneously record the β, γ and neutron activity from a radioactive source accumulated inside the detection system. For the TETRA optimization, series of the MCNP simulations were performed. Determination of the TETRA efficiency was done with ^{252}Cf spontaneous fission source based on multiplicity distribution of prompt neutrons confirming results of the MCNP simulations. However, during online experiments, based on recorded β–neutron-gated γ-spectra analysis, the efficiency measured was higher as compared to fast fission neutron of ^{252}Cf. According to the MCNP calculations, the efficiency, determined for delayed neutrons, showed that typical neutron energy did not exceed 0.5 MeV. It illustrates the fact that average delayed neutron energy in our experiment was low.

Furthermore, the TETRA integrated acquisition system is free from any dead time, which makes TETRA a tool of choice for detection of high-multiplicity neutron events. This feature will be important for the upcoming experiments with beams of neutron-rich nuclei, as with increasing large Q_β values the probability for multineutron emission channel increases. We have also demonstrated the ability of TETRA to be used as neutron trigger for β-decay γ-spectroscopy in spite of the inherently slow neutron registration process. Verification of the detection system was done in a commissioning experiment with a selectively photo-ionized ^{82}Ga beam confirming well-established already available in the literature. In the second experiment at mass 83, we obtained a P_n value for ^{83}Ga significantly higher than previously reported. Today, there is discrepancy between the experimentally measured data and predictions of existed theoretical approaches in the region which has to be understood.

The TETRA is currently based at ALTO (IPN, Orsay) to investigate structure and β-decay properties of neutron-rich r-process nuclei in vicinity of closed neutron shells $N = 50$, $N = 82$, but can be installed at any excising and future radioactive beam facilities, where movable tape collector technique is applicable, such as SPIRAL2 at Ganil, which will open access to new more neutron-rich species.

Acknowledgements. The authors wish to acknowledge support from the bilateral agreement JINR–CNRS and the TETRA collaboration. Also, we want to acknowledge the support of the Russian Foundation for Basic Research, Grant No. 14-02-91053CNRSa and of the Projet International de Coopération Scientifique (PICS). We thank the technical staff of the Tandem/ALTO facility for their assistance with the experiments and for providing excellent-quality radioactive beams. Use of one Ge detector from the French-UK IN2P3-STFC Gamma Loan Pool is acknowledged.

REFERENCES

1. *M. Madurga, R. Surman, I. N. Borzov et al.* Phys. Rev. Lett. 109 112501 (2012).
2. *I. N. Borzov* Nucl. Phys. A 777 645 (2006).
3. *I. N. Borzov* Phys. Rev. C 71 065801 (2005).
4. *I. N. Borzov* Phys. Rev. C 67 14 (2003).
5. http://atom.kaeri.re.kr/, Korea Atomic Energy Research Institute Nuclear Data Evaluation Laboratory, November (2007).
6. *J. Pereira, P. Hosmer, G. Lorusso et al.* Nucl. Instr & Meth. A 618 275 (2010).
7. *M. B. Gòmez-Hornillos, J. Rissanen, J. Tain et al.* J. Phys. Conf. Series 312 052008 (2010).
8. *D. Testov, Ch. Briançon, S. Dmitriev et al.* J. Phys. Atom. Nucl. 72 1 (2009).
9. *A. Etilé et al.* To be submitted at Phys. Rev. C.
10. *F. Azaiez, S. Essabaa, F. Ibrahim, D. Verney* Nucl. Phys. News, 23 5 (2013).
11. *S. Essabaa et al.* Nucl. Instr & Meth. B 317 218 (2013).
12. *R. Li, J. Lassen, A. Teigelhfer et al.* Nucl. Instr & Meth. 308 74 (2013).
13. *M. C. Mhamed et al.* Nucl. Instr & Meth. B 266 4092 (2008).
14. *G. Ter-Akopian, A. Popeko, E. Sokol et al.* Nucl. Instr & Meth. A 190 119 (1981).
15. *A. Yeremin, A. Belozerov, M. Chelnokov et al.* Nucl. Instr & Meth. A 539 441 (2005).
16. *A. Svirikhin, Ch. Briançon, S. Dmitriev et al.* AIP Conf. Proc. 1175 297 (2009).
17. *A. Svirikhin, A. Isaev, A. Yeremin et al.* Instr & Exp. Tech. 54 644 (2011).
18. *Y. Pyatkov, D. Kamanin, W. Oertzen et al.* Europ. Phys. J. A 48 1 (2012).
19. *J. L. Brisa, R. Sellema, J. Artigesa* Internal Report, Institut de Physique Nucleaire 06-03 (2006).
20. *M. Dakowski, Y. Lazarev, V. Turchin et al.* Nucl. Instr & Meth. 113 195 (1973).
21. *E. Sokol, V. Smirnov, S. Lukyanov* Nucl. Instr & Meth. A 400 96 (1997).
22. *E. J. Axton, A. G. Bardell, S. J. Felgate et al.* Metrologia 21 181 (1985).
23. *A. S. Vorobyev, V. N. Dushin, F. -J. Hambsch* AIP Conf. Proc. 769 613 (2005).
24. LA-UR-03-1987, MCNP A General Monte Carlo N-Particle Transport Code, Version 5 (2003).
25. *D. Testov, E. Kuznetcova, J. Wilson* Preprint JINR E15-128 (2013).

26. *P. Möller, J. Nix, K. -L. Kratz* ADNDT 66 131 (1997).
27. *K. Heyde* Basci Ideas and Concepts in Nuclear Physics (Institute of Physics Publishing Bristol and Philadelphia, 1999).
28. http://root.cern.ch/drupal/
29. *J. W. Meadows* Phys. Rev. 157 1076 (1967).
30. *S. Shalev, G. Rudstam* Phys. Rev. Lett. 28 687 (1972).
31. *S. Shalev, G. Rudstam* Nucl. Phys. A 230 153 (1974).
32. *H. Franz, J. V. Kratz, K.-L. Kratz et al.* Phys. Rev. Lett. 33 859 (1974).
33. *P. L. Reeder, J. F. Wright, L. J. Alquist* Phys. Rev. C 15 2098 (1977).
34. *P. Hoff* Nucl. Phys. A 359 9 (1981).
35. *G. Rudstam, K. Aleklett, L. Sihver* ADNDT 53 1 (1993).
36. *P. L. Reeder, R. A. Warner, G. P. Ford, H. Willmes* Radiation Effects 94 93 (1986).
37. *E. Lund, P. Hoff, K. Aleklett et al.* Z. Phys. A 294 233 (1980).
38. *K. -L. Kratz, H. Gabelmann, P. Möller et al.* Z. Phys. A 340 419 (1991).
39. http://http://www.nndc.bnl.gov, (08/2013).
40. *J. A. Winger, K. P. Rykaczewski, C. J. Gross et al.* Phys. Rev. C 81 044303 (2010).
41. http://t2.lanl.gov/nis/molleretal/publications/rspeed2002.html
42. *P. Möller* Phys. Rev. C 67 055802 (2003).
43. http://wwwndc.jaea.go.jp/nucldata/
44. *J. A. Winger, S. V. Ilyushkin et al.* Phys. Rev. Lett. 102 142502 (2009).
45. *I. N. Borzov* EPJ Web of Conferences 38 12002 (2012).
46. Progress in Nuclear Energy 41 39 (2002).
47. *O. Perru, D. Verney, F. Ibrahim* Eur. Phys. J 28 307 (2006).
48. *G. Rudstam, E. Lund* Phys. Rev. C 13 321 (1976).
49. *P. L. Reeder, R. A. Warner, M.O. Edminston, R. L. Gill, A. Pietrowski* Proc. Am. Soc. Nucl. Chem. Meeting Chicago, 171 (1985).

Received on October 31, 2014.

Редактор *В. В. Булатова*

Подписано в печать 29.12.2014.
Формат 60 × 90/16. Бумага офсетная. Печать офсетная.
Усл. печ. л. 1,5. Уч.-изд. л. 2,0. Тираж 245 экз. Заказ № 58443.

Издательский отдел Объединенного института ядерных исследований
141980, г. Дубна, Московская обл., ул. Жолио-Кюри, 6.
E-mail: publish@jinr.ru
www.jinr.ru/publish/